LA-UR- 11-00821

Approved for public release; distribution is unlimited.

Title: Spin relaxation and linear-in-electric-field frequency shift in an arbitrary, time-independent magnetic field

Author(s): Steven M. Clayton

Intended for: Journal of Magnetic Resonance

Los Alamos
NATIONAL LABORATORY
EST. 1943

Los Alamos National Laboratory, an affirmative action/equal opportunity employer, is operated by the Los Alamos National Security, LLC for the National Nuclear Security Administration of the U.S. Department of Energy under contract DE-AC52-06NA25396. By acceptance of this article, the publisher recognizes that the U.S. Government retains a nonexclusive, royalty-free license to publish or reproduce the published form of this contribution, or to allow others to do so, for U.S. Government purposes. Los Alamos National Laboratory requests that the publisher identify this article as work performed under the auspices of the U.S. Department of Energy. Los Alamos National Laboratory strongly supports academic freedom and a researcher's right to publish; as an institution, however, the Laboratory does not endorse the viewpoint of a publication or guarantee its technical correctness.

Form 836 (7/06)

Spin relaxation and linear-in-electric-field frequency shift in an arbitrary, time-independent magnetic field

Steven M. Clayton

Department of Physics, University of Illinois, Urbana, IL, 61820

Abstract

A method is presented to calculate the spin relaxation times T_1, T_2 due to a non-uniform magnetic field, and the linear-in-electric-field precession frequency shift $\delta\omega_E$ when an electric field is present, in the diffusion approximation for spins confined to a rectangular cell. It is found that the rectangular cell geometry admits of a general result for T_1, T_2, and $\delta\omega_E$ in terms of the spatial cosine-transform components of the magnetic field. The result is applied to the case of a permanently-magnetized dipole impurity near the cell.

Keywords:

1. Introduction

An experiment to measure the neutron electric dipole moment (nEDM), to be installed at the FnPB beamline at Oak Ridge National Laboratory, will utilize a helium-3 comagnetometer in the central, superfluid-helium-filled measurement cell [1][2]. A non-zero EDM would manifest as a difference in the Larmor precession frequency when electric and magnetic fields are aligned versus anti-aligned. In the nEDM measurement, the helium-3, which also acts as neutron spin analyzer, will be used to correct for drifts in the magnetic field. The helium-3 polarization must remain high over the entire measurement period, $\sim$1000 seconds, as the helium atoms precess in the holding field and diffuse within a rectangular cell. Also, as there is a strong electric field $\vec{E}$ applied across the cell, a subtle effect, in which the interplay of the motional $\vec{v} \times \vec{E}$ field with gradients in the static magnetic field cause the precession frequency to shift linearly with $\vec{E}$ [3] and thereby falsely signal an EDM, must be well-understood or shown to be negligible. Design optimization of the experimental apparatus includes calculating the helium-3 spin relaxation times T_1 (longitudinal), T_2 (dephasing), and linear-in-electric-field frequency shift $\delta\omega_E$ due to given magnetic field non-uniformities.

Email address: sclayton@lanl.gov (Steven M. Clayton)

Present address: Los Alamos National Laboratory, PO Box 1663, MS H846, Los Alamos, NM, 87545

In this article, a method is shown to calculate these quantities in the diffusion approximation in a rectangular cell and for an arbitrary magnetic field. The starting point for the relaxation times is the Redfield theory of spin relaxation [4]. In second order perturbation theory these can be written, for a holding field in the z direction, as [5]

$$\frac{1}{T_1} = \gamma^2 \left(k_{xx}(\omega_0) + k_{yy}(\omega_0)\right), \tag{1}$$

$$\frac{1}{T_2} = \frac{1}{2T_1} + \gamma^2 k_{zz}(0), \tag{2}$$

where the spectral density is given in terms of magnetic field perturbations $h_i(t)$,

$$k_{ij}(\omega) = \frac{1}{2}\int_{-\infty}^{\infty} \langle h_i(t) h_j(t+\tau)\rangle \cos\omega\tau d\tau. \tag{3}$$

Here, the total field in each direction i is $H_i(t) = \langle H_i(t)\rangle + h_i(t)$, such that average perturbation $\langle h_i(t)\rangle = 0$, and $\omega_0 = \gamma\langle H_z(t)\rangle$ is the average spin precession frequency.

McGregor [6] calculated the ensemble average correlation of the field perturbations seen by a diffusing particle in the case of a time-independent, uniform gradient of H_z in the x-direction,

$$\langle h_z(t) h_z(t+\tau)\rangle = \left(\frac{\partial H_z}{\partial x}\right)^2 \langle x(t) x(t+\tau)\rangle, \tag{4}$$

resulting in an analytic expression for T_2 in a rectangular cell,

$$\frac{1}{T_2} = \frac{1}{2T_1} + \frac{\gamma^2 L^4}{120D}\left[\frac{\partial H_z}{\partial x}\right]^2. \tag{5}$$

We relax the requirement of uniform gradient and find, in the case of a rectangular prism cell, that T_1 and T_2 can be written in terms of the components of the 3D cosine transform of $h_q(\vec{r})$ over the cell volume. The same technique is applied to dressed spins [7], with uniform holding field and non-uniform dressing field, by mapping non-uniformities in the dressing field to equivalent non-uniformities in the holding field. In Section 3, a variation of the technique is used for the linear-in-electric-field frequency shift. Finally, in Section 4, the method is applied to compute the relaxation times and linear-in-electric-field frequency shift due to sources of magnetic field non-uniformities near the cell: magnetic dipole impurities in given orientations and positions, and an infinitely-long superconducting rod.

2. Correlation functions in the diffusion limit

The correlation function of h_i can be expressed as integrals over the cell volume weighted by the probability density $p(\vec{r}_0, t)$ that the particle is at $\vec{r}_0$ at

the initial time t_0, and the joint probability density $p(\vec{r}, t|\vec{r}_0, t_0)$ that a particle at $\vec{r}_0$ at time t_0 will be at $\vec{r}$ at time t. Thus, [6]

$$\langle h_i(t_0)h_i(t_0+\tau)\rangle = \int_V d\vec{r}_0 h_i(\vec{r}_0)p(\vec{r}_0, t_0)\int_V d\vec{r} h_i(\vec{r})p(\vec{r}, t_0+\tau|\vec{r}_0, t_0). \quad (6)$$

The particle density will be taken as uniform in the cell, $p(\vec{r}, t) = 1/V$. The joint probability is the solution to the diffusion equation,

$$\frac{\partial}{\partial t}p(\vec{r}, t|\vec{r}_0, t_0) = D\nabla^2 p(\vec{r}, t|\vec{r}_0, t_0), \quad (7)$$

subject to reflecting boundary conditions at the walls,

$$\nabla p(\vec{r}_S, t|\vec{r}_0, t_0)\cdot\hat{n} = 0, \quad (8)$$

where $\vec{r}_S \in S$ and $\hat{n}$ is normal to the wall. In a rotated coordinate system (x', y', z') aligned with the cell walls, the solution for a $L_x \times L_y \times L_z$ box with walls at $x' = \pm L_x/2$, $y' = \pm L_y/2$ and $z' = \pm L_z/2$ is

$$p(\vec{r}', t|\vec{r}_0', t_0) = p(x', t|x_0', t_0; L_x)p(y', t|y_0', t_0; L_y)p(z', t|z_0', t_0; L_z), \quad (9)$$

with the 1D solution dependent on the time difference $\tau = t - t_0$, [6]

$$\begin{aligned} p(x', t|x_0', t_0; L_x) &= \frac{1}{L_x} + \frac{2}{L_x}\sum_{n=1,3,\ldots}^{\infty} e^{-n^2\pi^2 D\tau/L_x^2}\sin\frac{n\pi x'}{L_x}\sin\frac{n\pi x_0'}{L_x} \\ &\quad + \frac{2}{L_x}\sum_{n=2,4,\ldots}^{\infty} e^{-n^2\pi^2 D\tau/L_x^2}\cos\frac{n\pi x'}{L_x}\cos\frac{n\pi x_0'}{L_x}. \end{aligned} \quad (10)$$

It will be convenient to recognize the following:

$$p(x'-L_x/2, t|x_0'-L_x/2, t_0; L_x) = \frac{1}{L_x} + \frac{2}{L_x}\sum_{n=1,2,3,\ldots}^{\infty} e^{-n^2\pi^2 D\tau/L_x^2}\cos\frac{n\pi x'}{L_x}\cos\frac{n\pi x_0'}{L_x}. \quad (11)$$

Putting Eq. 9 and $p(\vec{r}_0', t_0) = 1/V$ into Eq. 6, changing the limits of integration to $0 \le q_i' \le L_i$ for each dimension q_i' and using Eq. 11, we have

$$\begin{aligned} g_{ii}(\tau) &= \langle h_i(t_0)h_i(t_0+\tau)\rangle \\ &= \sum_{n_x,n_y,n_z=0}^{\infty} e^{-\pi^2 D(n_x^2/L_x^2+n_y^2/L_y^2+n_z^2/L_z^2)\tau} \\ &\quad \times\frac{1}{V}\int_{V'} dx_0'\,dy_0'\,dz_0'\,h_i(x_0'-L_x/2, y_0'-L_y/2, z_0'-L_z/2) \\ &\quad C_{n_x}C_{n_y}C_{n_z}\cos\frac{n_x\pi x_0'}{L_x}\cos\frac{n_y\pi y_0'}{L_y}\cos\frac{n_z\pi z_0'}{L_z} \\ &\quad \times\frac{1}{V}\int_{V'} dx'\,dy'\,dz'\,h_i(x'-L_x/2, y'-L_y/2, z'-L_z/2) \\ &\quad C_{n_x}C_{n_y}C_{n_z}\cos\frac{n_x\pi x'}{L_x}\cos\frac{n_y\pi y'}{L_y}\cos\frac{n_z\pi z'}{L_z} \end{aligned} \quad (12)$$

in which the factor C_n has been introduced,

$$C_n = \begin{cases} 1 & \text{if } n = 0 \\ \sqrt{2} & \text{otherwise.} \end{cases} \tag{13}$$

We identify the 3D cosine transform of $h_i(\vec{r}')$ within Eq. 12,

$$\begin{aligned} \mathcal{A}^{\vec{n}}\{h_i\} &\equiv \frac{1}{V}\int_{V'} dx'\,dy'\,dz'\,h_i(x'-L_x/2, y'-L_y/2, z'-L_z/2) \\ &\quad \times \cos\frac{n_x\pi x'}{L_x}\cos\frac{n_y\pi y'}{L_y}\cos\frac{n_z\pi z'}{L_z}, \end{aligned} \tag{14}$$

(where the integral is over the range $x' \in [0, L_x]$, $y' \in [0, L_y]$, $z' \in [0, L_z]$), giving finally

$$g_{ii}(\tau) = \sum_{n_x,n_y,n_z=0}^{\infty} e^{-\tau/\tau_c^{\vec{n}}} C_{n_x}^2 C_{n_y}^2 C_{n_z}^2 \left(\mathcal{A}^{\vec{n}}\{h_i\}\right)^2, \tag{15}$$

with the characteristic time τ_c for a given spatial mode defined by

$$\frac{1}{\tau_c^{\vec{n}}} = \pi^2 D\left(\frac{n_x^2}{L_x^2} + \frac{n_y^2}{L_y^2} + \frac{n_z^2}{L_z^2}\right) \tag{16}$$

Putting this expression into Eq. 3 and performing the integral over τ gives

$$k_{ii}(\omega) = \sum_{n_x,n_y,n_z=0}^{\infty} C_{n_x}^2 C_{n_y}^2 C_{n_z}^2 \frac{\tau_c^{\vec{n}}}{1+\omega^2(\tau_c^{\vec{n}})^2}\left(\mathcal{A}^{\vec{n}}\{h_i\}\right)^2, \tag{17}$$

Substitution into Eqs. 1 and 2 results in complete expressions for the longitudinal and transverse relaxation times.

2.1. Extension to dressed spins with non-uniform dressing field

An RF magnetic field with amplitude B_1 applied transverse to the holding field B_0 modifies the effective precession frequency of a particle. In terms of dimensionless dressing parameters

$$X = \frac{\gamma B_1}{\omega_{\text{RF}}},\ Y = \frac{\gamma B_0}{\omega_{\text{RF}}}, \tag{18}$$

in the limit $Y \ll 1$ the effective gyromagnetic ratio becomes [7]

$$\gamma_{\text{eff}} = \gamma J_0(X). \tag{19}$$

Thus for a dressing field with spatially varying amplitude $B_1(\vec{r}) = \langle B_1\rangle + \delta B_1(\vec{r})$, the equivalent variation $\delta\tilde{B}_0$ in the holding field B_0 is given by [1]

$$\gamma_{\text{eff}}\delta\tilde{B}_0 \leftrightarrow \delta\gamma_{\text{eff}}B_0 = B_0\frac{\partial\gamma_{\text{eff}}}{\partial X}\delta X = B_0\gamma J_1(X)\delta X, \tag{20}$$

The expressions from the previous sections can be used to calculate T_2 for the dressed spin with a non-uniform dressing field by setting

$$\gamma \rightarrow \gamma_{\text{eff}}, \tag{21}$$

$$\omega_0 \rightarrow \gamma_{\text{eff}} B_0, \tag{22}$$

$$h_z(\vec{r}) \rightarrow Y \frac{J_1(X)}{J_0(X)} \delta B_1(\vec{r}) + \delta B_0(\vec{r}), \tag{23}$$

where any variation δB_0 in the holding field itself has been included in h_z.

3. Linear electric field frequency shift

A spin moving though an electric field experiences a motional magnetic field that may, in conjunction with gradients of the magnetic field, produce a shift in the precession frequency dependent on the electric field direction and magnitude [3]. Of particular concern in searches for electric dipole moments are effects that are linearly proportional to the electric field E. These may mimic effects expected for an electric dipole moment, thereby creating a "false EDM."

As shown by Lamoreaux and Golub [8], the linear-in-electric-field frequency shift for spins in a confined volume is given by the expression

$$\delta\omega_E = -\frac{1}{2}\int_0^t d\tau \, \cos\omega_0\tau \{\langle \omega_x(t)\omega_y(t-\tau)\rangle - \langle \omega_x(t-\tau)\omega_y(t)\rangle\}, \tag{24}$$

where the perturbations can be written more generally as

$$\omega_x(t) = \gamma h_x(t) + \gamma \frac{E}{c} v_y(t), \quad \omega_y(t) = \gamma h_y(t) - \gamma \frac{E}{c} v_x(t). \tag{25}$$

Expanding the expression for $\delta\omega_E$ and keeping only terms linear in E results in

$$\begin{aligned} \delta\omega_E &= \frac{\gamma^2 E}{2c}\int_0^t d\tau \, \cos\omega_0\tau \{\langle h_y(t)v_y(t-\tau)\rangle + \langle h_x(t)v_x(t-\tau)\rangle \\ &\quad -\langle h_y(t-\tau)v_y(t)\rangle - \langle h_x(t-\tau)v_x(t)\rangle\}. \end{aligned} \tag{26}$$

The cosine-transform method developed in the present work can be used to compute Eq. 26 in the diffusion limit for the nEDM cell geometry. While the expressions,

$$y(t) = y_0 + \int_0^t v_y(t')dt', \quad y(t-\tau) = y_0 + \int_0^{t-\tau} v_y(t')dt', \tag{27}$$

were used in Ref. [8] to eliminate y in favor of an expression with v_y, here we remove the velocity components from the correlation functions and use instead the Fundmental Theorem of Calculus and the above expression for $y(t-\tau)$. The correlation functions can then be written

$$\langle h_y(t)v_y(t-\tau)\rangle = -\frac{\partial}{\partial\tau}\langle h_y(t)y(t-\tau)\rangle, \tag{28}$$

$$\langle h_y(t-\tau)v_y(t)\rangle = \langle h_y(t)v_y(t+\tau)\rangle = \frac{\partial}{\partial\tau}\langle h_y(t)y(t+\tau)\rangle. \tag{29}$$

In the latter expression, averages are assumed to be independent of the overall time offset t, as appropriate for a stationary problem.

The expressions in Section 2 are modified to give the correlation function in the diffusion limit in terms of the cosine-transform components of $h_y(\vec{r})$ and $y(\vec{r})$,

$$\langle h_y(t)y(t-\tau)\rangle = \sum_{n_x,n_y,n_z} e^{-\tau/\tau_c^{\vec{n}}} C_{n_x}^2 C_{n_y}^2 C_{n_z}^2 \mathcal{A}^{\vec{n}}\{h_y\}\,\mathcal{A}^{\vec{n}}\{y\}. \tag{30}$$

$$\langle h_y(t)v_y(t-\tau)\rangle = \sum_{n_x,n_y,n_z} \frac{1}{\tau_c^{\vec{n}}} e^{-\tau/\tau_c^{\vec{n}}} C_{n_x}^2 C_{n_y}^2 C_{n_z}^2 \mathcal{A}^{\vec{n}}\{h_y\}\,\mathcal{A}^{\vec{n}}\{y\} \tag{31}$$

Performing the integral in Eq. 26, we have

$$\int_0^\infty d\tau\, \cos\omega_0\tau\langle h_y(t)v_y(t-\tau)\rangle = \sum_{n_x,n_y,n_z} \frac{1}{1+(\omega_0\tau_c^{\vec{n}})^2} C_{n_x}^2 C_{n_y}^2 C_{n_z}^2 \mathcal{A}^{\vec{n}}\{h_y\}\,\mathcal{A}^{\vec{n}}\{y\}, \tag{32}$$

leading to an expression for the frequency shift,

$$\delta\omega_E = \frac{\gamma^2 E}{c} \sum_{n_x,n_y,n_z} \frac{1}{1+(\omega_0\tau_c^{\vec{n}})^2} C_{n_x}^2 C_{n_y}^2 C_{n_z}^2 \left[\mathcal{A}^{\vec{n}}\{h_y\}\,\mathcal{A}^{\vec{n}}\{y\} + \mathcal{A}^{\vec{n}}\{h_x\}\,\mathcal{A}^{\vec{n}}\{x\}\right]. \tag{33}$$

The summation can be reduced by computing the cosine transform components of $x(\vec{r})$ and $y(\vec{r})$ analytically,

$$\mathcal{A}^{\vec{n}}\{x\} = \begin{cases} -\frac{2L_x}{n_x^2\pi^2} & \text{if } n_x = 1,3,\ldots; n_y = n_z = 0 \\ 0 & \text{otherwise.} \end{cases} \tag{34}$$

The result for the frequency shift in the diffusion approximation is

$$\delta\omega_E = \frac{4\gamma^2 E}{c}\left[\sum_{n_y=1,3,\ldots} \frac{L_y}{n_y^2\pi^2} \frac{\mathcal{A}^{(0,n_y,0)}\{h_y\}}{1+(\omega_0\tau_c^{(0,n_y,0)})^2} + \sum_{n_x=1,3,\ldots} \frac{L_x}{n_x^2\pi^2} \frac{\mathcal{A}^{(n_x,0,0)}\{h_x\}}{1+(\omega_0\tau_c^{(n_x,0,0)})^2}\right]; \tag{35}$$

we are left with 1-dimensional cosine transforms of the field perturbation in x and y. The false EDM equivalent to this linear-in-electric-field shift is

$$d_{v\times E} = \frac{2\hbar}{E}\delta\omega_E. \tag{36}$$

4. Example applications

The bulk of the computational effort required for practical application of the present technique is in finding the cosine transform amplitudes $\mathcal{A}^{\vec{n}}$ of the field non-uniformities. The form of Eq. 14 is amenable to numerical computation with Fast Fourier Transform software libraries. The examples below use the

multidimensional discrete cosine transform (DCT) feature of the freely-available software library FFTW3 [9]. Input to the DCT for each field component is an array of field perturbations $h_q(\vec{r})$ sampled over the cell volume at $N_x \times N_y \times N_z$ grid points, and the output is an array of DCT amplitudes which, after scaling by $1/(8N_xN_yN_z)$, correspond to the desired amplitudes $\mathcal{A}^{\vec{n}}$. The summations in Eqs. 17 and 35 are truncated according to the amplitudes available from the DCT. Accuracy of the result can be checked by increasing the number of sample points and repeating the computation. Note that for the linear-in-electric-field frequency shift (false-EDM) result, each of the two terms in Eq. 35 requires only a 1-dimensional cosine transform of the respective field perturbation component averaged over the other dimensions.

4.1. Dipole source near the cell

We calculate the effect of a magnetic dipole source, here a small, permanently-magnetized sphere of radius a, placed near the cell in an otherwise uniform field. The field perturbation at a point $\vec{r}$ with respect to the center of the sphere is [10]

$$\vec{B}_d(\vec{r}) = B_s \left(\frac{a}{r}\right)^3 \frac{1}{2}(3\hat{n}\cdot\hat{m}\,\hat{n} - \hat{m}), \quad |\vec{r}| \geq a, \tag{37}$$

where B_s is the magnitude of the field on the surface of the sphere at its poles, $\hat{m}$ is the unit vector in the direction of the magnetization, and $\hat{n}$ is the unit vector along $\vec{r}$.

The cell in this study has dimensions $L_x = 10.2$ cm, $L_y = 50$ cm, $L_z = 7.6$ cm and contains a dilute mixture of helium-3 in helium-4 at 450 mK, for a helium-3 diffusion constant of $D = 428$ cm^2/s [11]. The 10-mG, uniform holding field is in the z-direction, and four different dipole impurity cases are considered all with $B_s = 1$ Tesla: Dipole Source A, with diameter 150 μm, location $\vec{r}_d = (0, 0, 5.07)$ cm, orientation $\hat{m}$ along the z-axis; Dipole Source B, with diameter 150 μm, location $\vec{r}_d = (5.00, 25.00, 5.07)$ cm, orientation $\hat{m}$ along the z-axis; Dipole Source C, with diameter 175 μm, location $\vec{r}_d = (0, 0, 5.07)$ cm, orientation $\hat{m}$ along the x-axis; and Dipole Source D, with diameter 175 μm, location $\vec{r}_d = (5.00, 25.00, 5.07)$ cm, orientation $\hat{m}$ along the x-axis. The location $\vec{r}_d$ given for each dipole is with respect to an origin at the center of the cell volume and corresponds to an outside face of a 1.27-cm-thick cell wall, either at the center of the face (Sources A and C) or near the corner (Sources B and D). The results for relaxation times T_1, T_2, and false EDM due to the magnetic field nonuniformity are shown in Table 4.1. The calculation was repeated for several different numbers of grid points used in the discrete cosine transform over the cell volume, and stability of the results is evident as the grid is made increasingly fine.

The prediction for T_2 due to each dipole source was checked by a diffusion Monte Carlo simulation. The simulated particles were treated classically, with constant velocity consistent with the thermal average kinetic energy of helium-3 quasiparticles, and with the scattering mean free path set consistent with the diffusion constant. At a temperature of 450 mK, this gives a mean free

Case	$N_x \times N_y \times N_z$	T_1 (s)	T_2 (s)	$d_{v \times E}$
Dipole source A	$64 \times 256 \times 32$	4467.65	830.59	-5.0622e-27
Dipole source A	$64 \times 512 \times 32$	4467.65	830.59	-5.0622e-27
Dipole source A	$64 \times 512 \times 64$	4444.89	829.15	-5.0784e-27
Dipole source A	$128 \times 512 \times 64$	4444.90	829.16	-5.0824e-27
Dipole source A	$128 \times 512 \times 128$	4439.24	828.80	-5.0865e-27
Dipole source B	$64 \times 256 \times 32$	16967.75	3286.58	-1.5089e-27
Dipole source B	$64 \times 512 \times 32$	16987.42	3286.95	-1.4836e-27
Dipole source B	$64 \times 512 \times 64$	16864.89	3280.61	-1.5207e-27
Dipole source B	$128 \times 512 \times 64$	16878.04	3280.85	-1.5044e-27
Dipole source B	$128 \times 512 \times 128$	16847.56	3279.27	-1.5137e-27
Dipole source C	$64 \times 256 \times 32$	3487.66	993.46	-8.8261e-43
Dipole source C	$64 \times 512 \times 32$	3487.66	993.46	-1.1026e-42
Dipole source C	$64 \times 512 \times 64$	3470.03	990.81	-1.0648e-42
Dipole source C	$128 \times 512 \times 64$	3470.09	990.85	-1.3352e-42
Dipole source C	$128 \times 512 \times 128$	3465.71	990.19	-1.3549e-42
Dipole source D	$64 \times 256 \times 32$	14022.45	642.52	2.0254e-26
Dipole source D	$64 \times 512 \times 32$	14027.46	642.52	2.0274e-26
Dipole source D	$64 \times 512 \times 64$	13947.02	641.22	2.0287e-26
Dipole source D	$128 \times 512 \times 64$	13950.38	641.69	2.0288e-26
Dipole source D	$128 \times 512 \times 128$	13930.38	641.36	2.0292e-26

Table 1: Results of the calculation for the different combinations of dipole source location, orientation, and strength described in the text, and for several discrete cosine transform grid sizes. The parameters of each dipole source are given in the text.

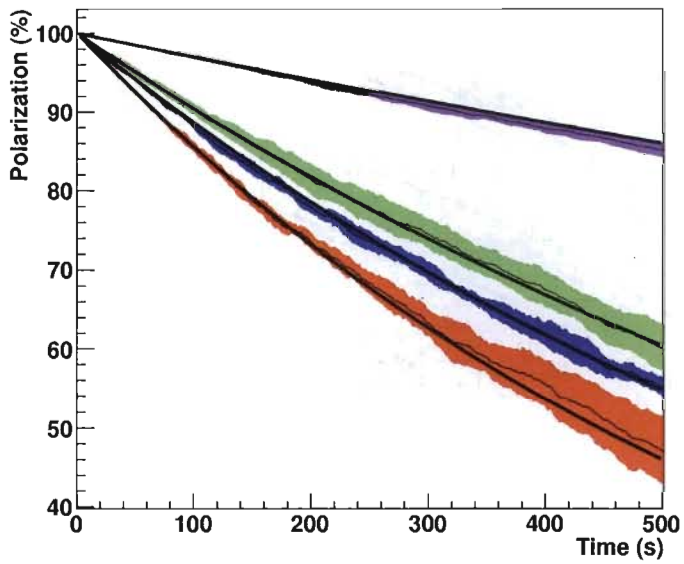

Figure 1: Results for the transverse polarization $P(t)$ versus time from the diffusion Monte Carlo simulations for T_2 due a a dipole source near the cell. The shaded bands indicate the standard deviation of five curves $P(t)$ for each dipole source found by subdividing the ensemble of 2000 simulated particles. In order from shortest to longest T_2, the curves are for Dipole Sources D, A, C, and B described in the text. The smooth black lines are the predicted $P(t) = \exp(-t/T_2^{\rm th})$, where $T_2^{\rm th}$ for each dipole source is taken from Table 4.1.

path of 3.54 mm, sufficiently small compared to the cell dimensions that the diffusion approximation is expected to be valid. Each simulated particle was started with spin initially aligned with the y-axis (transverse to the 10-mG holding field), and the spin orientation ($\vec{S}_i$ for particle i) as the particle moved throughout the cell volume was evolved in the Rotating Frame [5] using a Runge-Kutta method with adaptive stepsize control [12]. For each dipole source, 2000 helium-3 particles were simulated, and the polarization in the plane transverse to the holding field was found from the vector sum of spin directions versus time, $P(t) = \left|\sum_i \vec{S}_i^{\rm tr}(t)/n\right|$, where $\vec{S}_i^{\rm tr}$ is the projection of spin i onto the plane transverse to the holding field. Simulation results are shown in Fig. 1 along with predictions from the present technique, demonstrating good agreement between the simulation and theory calculation.

The cosine-transform technique is also applied in turn to Dipole Sources A through D repositioned successively further away from the cell in the z-direction. Results are shown in Fig. 2 for the dipole source located as close as the outside of the 1.27-cm-thick cell wall. Dipole sources much closer than the outside of the cell wall are not considered here because the rapidly-falling field very near the

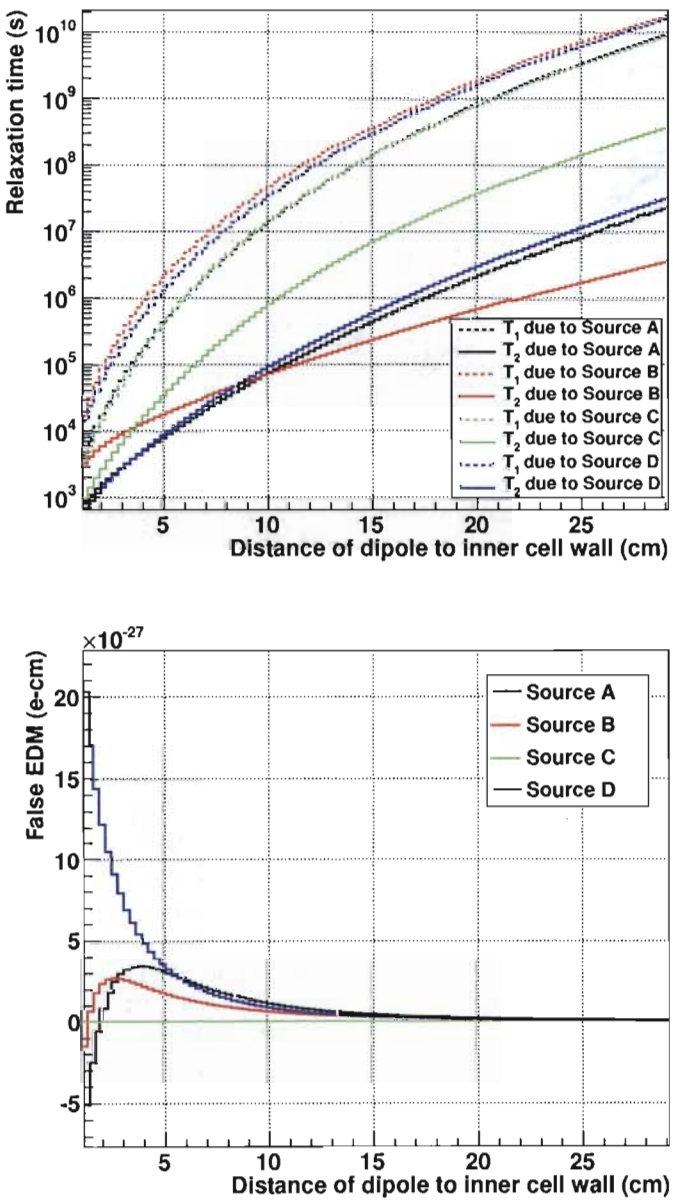

Figure 2: Calculated relaxation times and false EDM arising from Dipole Sources A through D described in the text, as the sources are repositioned further away from the cell in the z-direction. The number of grid points in the discrete cosine transform over the $L_x \times L_y \times L_z = 10.2 \times 50 \times 7.6$ cm^3 cell is $N_x \times N_y \times N_z = 128 \times 512 \times 128$.

source would not be well-represented by a 3-dimensional DCT over a practical number of grid points. As long as the average magnetic field perturbation remains small compared to the holding field, the results may be scaled to other dipole strengths: $T_{1,2} \propto (B_s a^3)^2$ and $d_{v\times E} \propto B_s a^3$. Dipole Source C, centered above the cell and oriented in the x-direction, gives zero (within numerical precision) false EDM because h_x is symmetric across $x = 0$, and h_y is symmetric across $y = 0$; i.e., there are no odd components in the cosine transform of these perturbations in their respective directions.

4.2. Superconducting rod near the cell

As another example, we calculate the effect of a superconducting rod placed near the cell in an otherwise uniform holding field. For an infinite-length rod along the y axis and through the origin in a magnetic field B_0 applied along the z axis, the net field around the rod is [13]

$$B_\rho = (1 - \frac{a^2}{\rho^2}) B_0 \cos\phi, \tag{38}$$

$$B_\phi = (1 + \frac{a^2}{\rho^2}) B_0 \sin\phi, \tag{39}$$

where a is the rod radius and (ρ, ϕ) are polar coordinates in the zx plane. While the cosine transforms of B_x, B_z derived from these equations (appropriately translated to the desired location of the superconducting rod) could perhaps be calculated analytically, here the equations are used to generate a field map that is subsequently run through the machinery to produce values for T_1, T_2, and $d_{v\times E}$. Results are shown in Figure 3, with physical parameters given in the caption.

5. Conclusion

A method to calculate spin relaxation times and the linear-in-electric-field frequency shift in the diffusion approximation was presented. The technique is based on the observation that, for particles diffusing in a rectangular cell, the correlation function of position-dependent fields experienced by the particles is the weighted sum over the product of spatial cosine-transform components of the fields.[3] As the formulation is intended for practical computation in a rectagular cell, the result is for the complete 3-dimensional geometry. In the linear-in-electric-field frequency shift calculation, the non-zero terms in the summation amount to 1-dimensional cosine transforms in the directions transverse to the holding field; this is discussed further in Appendix A, where the dipole impurity

[3]During preparation of this manuscript, independent work was published based on essentially the same observation for the T_1, T_2 calculation. These authors point out that their result may be used as a probe for possible unknown spin interactions and applied it to improve the limits on axion-like interactions with the cell walls [14].

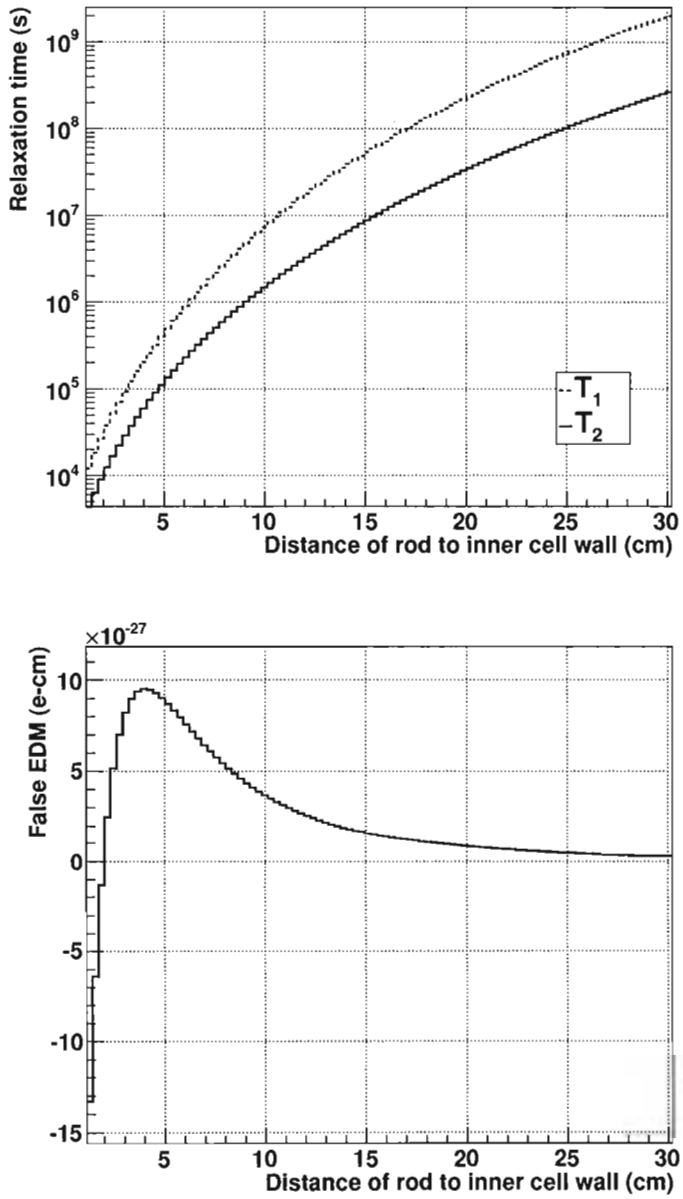

Figure 3: Calculated relaxation times $T1$, $T2$ and false EDM $d_{v\times E}$ due to the magnetic field distortion from a 3-mm-diameter, infinitely-long superconducting rod parallel to the y-axis and placed near the cell. The rod is centered over the cell in the x-direction, and the horizontal axis of the plots is the distance along the z-axis between the inside of the cell wall and the center of the rod. The parameters are diffusion constant $D = 428$ cm^2/s (corresponding to a temperature of 450 mK [11]), holding field $B_0 = 10$ mG (applied parallel to the z-axis), and cell dimensions $L_x = 10.2$ cm, $L_y = 50$ cm, $L_z = 7.6$ cm.

example is extended. Computation of the relaxation times requires in general the full 3-dimensional cosine transform. Practical computation is done using fast discrete cosine transforms of the field components.

In addition to evaluating the effect of magnetic impurities near the cell as in the above examples, this method could be used in magnet coil design optimization: given a field map, T_1, T_2, and $\delta\omega_E$ can be quickly evalulated and combined into a figure of merit.

6. Acknowledgements

This work was supported by NSF grant number NSF06-01067. The author thanks R. Golub for suggesting the application to the linear-in-electric-field frequency shift.

Appendix A. $\delta\omega_E$ due to a magnetic dipole impurity

In the expression for the linear-in-electric-field frequency shift, Eq. 35, the full 3-dimensional cosine transform is not required. Integrating over the zero-mode directions in $\mathcal{A}^{(n_x,0,0)}\{h_x\}$ leaves a 1-dimensional cosine transform in the remaining direction,

$$\mathcal{A}^{(n_x,0,0)}\{h_x\} = \mathcal{A}^{n_x}\{\frac{1}{L_y L_z}\int_A h_x\, dy\, dz\}, \tag{A.1}$$

where A is the cross-sectional area of the cell in the yz-plane, and

$$\mathcal{A}^{n_x}\{f\} \equiv \frac{1}{L_x}\int_0^{L_x} dx'\, f(x'-L/2)\cos\frac{n\pi x'}{L}. \tag{A.2}$$

It remains to calculate h_x averaged over yz-plane cross sections and similarly for h_y, i.e., the total magnetic flux through these cross sections divided by area. The analytic expression developed in this appendix for a dipole impurity near the cell, illustrated in Fig. A.4, is also applicable to the problem of finding the magnetic flux due to a dipole through a piecewise linear pickup loop.

The magnetic flux through a surface S due to a dipole $\vec{m}$ at point $\vec{r}_m$ is

$$\Phi(\vec{r}_m) = \int_S \vec{B}(\vec{r}-\vec{r}_m)\cdot d\vec{a} = \int_S \left(\vec{\nabla}_r \times \vec{A}(\vec{r}-\vec{r}_m)\right)\cdot d\vec{a} = \oint_{\partial S} \vec{A}(\vec{r}-\vec{r}_m)\cdot d\vec{l}. \tag{A.3}$$

The magnetic vector potential at point $\vec{r}$ due to a dipole $\vec{m}$ at point $\vec{r}_m$ is

$$\vec{A}(\vec{r}-\vec{r}_m) = \frac{\mu_0}{4\pi}\frac{\vec{m}\times(\vec{r}-\vec{r}_m)}{|\vec{r}-\vec{r}_m|^3}. \tag{A.4}$$

In terms of the maximum surface field B_s of a spherical, uniformly and permanently magnetized impurity of radius a, the dipole strength is

$$|\vec{m}| = \frac{2\pi B_s a^3}{\mu_0}. \tag{A.5}$$

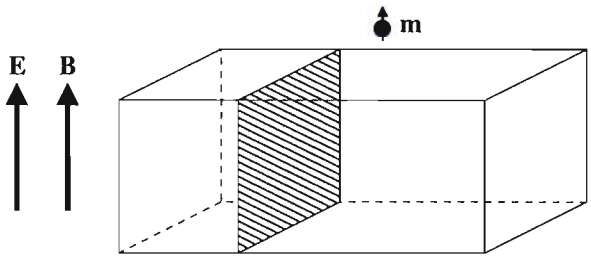

Figure A.4: Diagram of the cell configuration, indicating the impurity dipole $\vec{m}$ and one of the cell cross-sections over which the average field perturbation due to the dipole is calculated.

Consider a closed planar surface S bounded by N connected line segments which have successive endponts $\vec{a}_i$, $i = 0, ..., N$ and $\vec{a}_N = \vec{a}_0$. We will explicitly calculate the contribution $\Delta\Phi_i$ to the line integral Eq. A.3 from the boundary line segment extending from $\vec{a}_i$ to $\vec{a}_{i+1}$, then sum over all segments to get the total flux due to the dipole.

$$\Delta\Phi_i(\vec{r}_m) = \int_{\vec{a}_i}^{\vec{a}_{i+1}} \vec{A}(\vec{r} - \vec{r}_m) \cdot d\vec{l} = \frac{\mu_0}{4\pi} \int_{\vec{a}_i}^{\vec{a}_{i+1}} \frac{\vec{m} \times (\vec{r} - \vec{r}_m)}{|\vec{r} - \vec{r}_m|^3} \cdot d\vec{l} \tag{A.6}$$

The line from $\vec{a}_i$ to $\vec{a}_{i+1}$ can be parameterized in terms of a scalar $t \in [-1, 1]$,

$$\vec{L}_i \equiv \vec{a}_{i+1} - \vec{a}_i \tag{A.7}$$

$$\vec{R}_i \equiv \frac{1}{2}(\vec{a}_i + \vec{a}_{i+1}) - \vec{r}_m \tag{A.8}$$

$$\vec{l} = \vec{R}_i + \frac{1}{2} t \vec{L}_i, \tag{A.9}$$

$$d\vec{l} = \frac{1}{2} dt \vec{L}_i. \tag{A.10}$$

Equation A.6 becomes

$$\Delta\Phi_i = \frac{\mu_0}{4\pi} \int_{\vec{a}_i - \vec{r}_m}^{\vec{a}_{i+1} - \vec{r}_m} \frac{\vec{m} \times \vec{l}}{l^3} \cdot d\vec{l} \tag{A.11}$$

$$= \frac{\mu_0}{4\pi} \int_{-1}^{1} dt \frac{\vec{m} \times (\vec{R}_i + t\vec{L}_i/2) \cdot \vec{L}_i/2}{(R_i^2 + t\vec{R}_i \cdot \vec{L}_i/2 + t^2 \vec{L}_i^2/4)^{3/2}} \tag{A.12}$$

$$= \frac{\mu_0 \vec{m} \times \vec{R}_i \cdot \vec{L}_i}{8\pi R_i^3} \int_{-1}^{1} \frac{dt}{(1 + t\vec{R}_i \cdot \vec{L}_i/(2R_i^2) + t^2 L_i^2/(4R_i^2))^{3/2}} \tag{A.13}$$

The solution to the integral ([15], Eq. 2.263.3),

$$\int_{-1}^{1} \frac{dt}{(1 + 2bt + c^2t^2)^{3/2}} = \left. \frac{b + c^2 t}{(c^2 - b^2)\sqrt{1 + 2bt + c^2t^2}} \right|_{-1}^{1} \tag{A.14}$$

$$= \frac{c^2 - b}{(c^2 - b^2)\sqrt{1 - 2b + c^2}} + \frac{c^2 + b}{(c^2 - b^2)\sqrt{1 + 2b + c^2}} \tag{A.15}$$

yields an algebraic expression for $\Delta\Phi_i$, and the flux through the loop is found by summation over all of its constituent line segments.

The average h_x and h_y can now be evaluated at discrete points along x and y, respectively, and fed into 1-dimensional discrete cosine transforms. Results using this method, rather than the full 3-dimensional cosine transform as required for T_1 and T_2, are shown in Fig. A.5 for a dipole source scanned over the outer cell wall.

References

[1] R. Golub, S. Lamoreaux, Neutron electric-dipole moment, ultracold neutrons and polarized ^{3}He, Phys. Rep. 237 (1994) 1.

[2] Neutron EDM Collaboration, *Los Alamos National Laboratory Technical Report* LA-UR 02-2331, 2002.

[3] J. M. Pendlebury, et al., Geometric-phase-induced false electric dipole moment signals for particles in traps, Phys. Rev. A 70 (2004) 032102.

[4] A. G. Redfield, IBM J. Res. Dev. 1 (1957) 19.

[5] C. P. Slichter, Principles of magnetic resonance, 3rd ed., Springer-Verlag, 1996.

[6] D. D. McGregor, Transverse relaxation of spin-polarized ^{3}He gas due to a magnetic field gradient, Phys. Rev. A41 (1990) 2631.

[7] C. Cohen-Tannoudji, S. Haroche, Absorption and scattering of optical photons by an atom interacting with radiofrequency photons, Journal de Physique 30 (1969) 153.

[8] S. K. Lamoreaux, R. Golub, Detailed discussion of a linear electric field frequency shift induced in confined gases by a magnetic field gradient: Implications for neutron electric-dipole-moment experiments, Phys. Rev. A71 (2005) 032104.

[9] M. Frigo, S. G. Johnson, The design and implementation of FFTW3, Proc. IEEE 93 (2) (2005) 216–231.

[10] J. D. Jackson, Classical Electrodynamics, 2nd ed., John Wiley & Sons, Inc., 1975.

[11] S. K. Lamoreaux, et al., Measurement of the ^{3}He mass diffusion coefficient in superfluid ^{4}He over the 0.45—0.95 K temperature range, Europhys. Lett. 58 (5) (2002) 718–724.

[12] W. H. Press, S. A. Teukolsky, W. T. Vetterling, B. P. Flannery, Numerical Recipes, 2nd ed., Cambridge University Press, 1992.

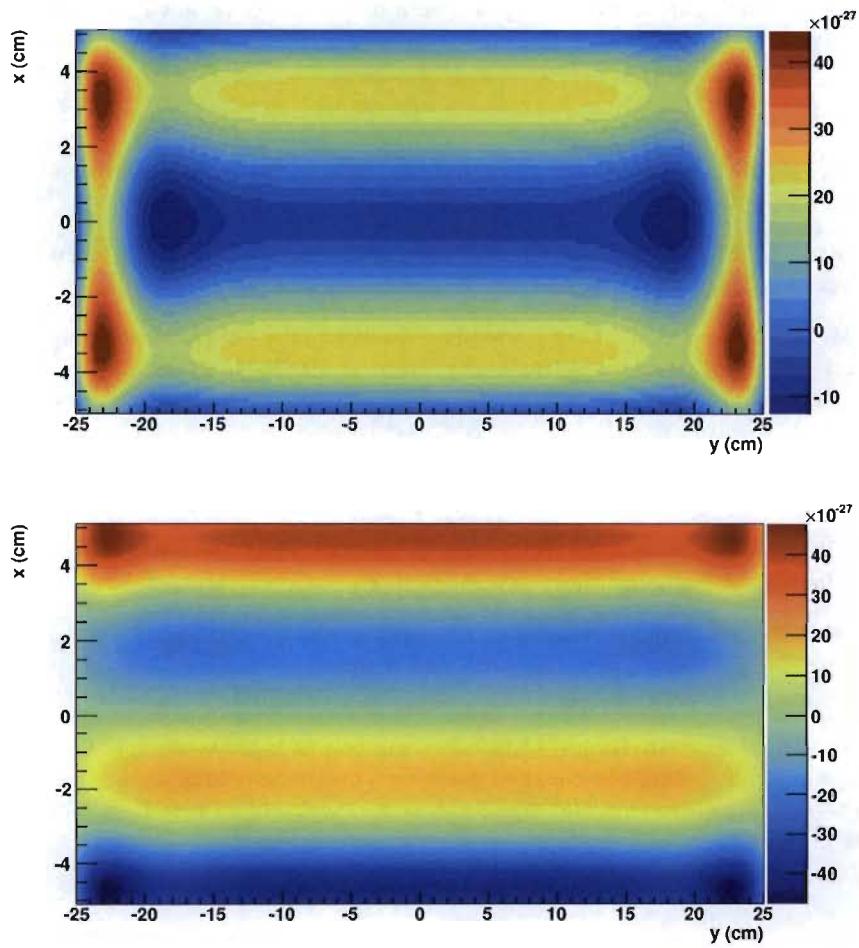

Figure A.5: Results for the false-EDM effect (in e−cm) due to a dipole impurity 1.27 cm above the $L_x \times L_y \times L_z = 10.2 \times 50 \times 7.6$ cm^3 cell, versus the position of the dipole in the axes transverse to the holding field. For the upper plot, the dipole source is aligned with the z-axis (holding field direction), has radius $a = 150$ μm and maximum surface field $B_s = 1$ T. For the lower plot, the dipole source is aligned with the x-axis, has $a = 175$ μm and $B_s = 1$ T.

[13] C. P. Poole, H. A. Farach, R. J. Creswick, Superconductivity, 2nd ed., Academic Press, 2007.

[14] A. K. Petukhov, G. Pignol, D. Jullien, K. H. Andersen, Polarized ^3He as a probe for short-range spin-dependent interactions, Phys. Rev. Lett. 105 (17) (2010) 170401.

[15] I. S. Gradshteyn, I. M. Ryzhik, Table of Integrals, Series, and Products, 5th ed., Academic Press, 1994.